A Hypothalamic-Controlled Neural Reflex Promotes Corneal Inflammation

Romina Mayra Lasagni Vitar,[1] Philippe Fonteyne,[1] Linda Chaabane,[2] Paolo Rama,[1] and Giulio Ferrari[1]

[1]Cornea and Ocular Surface Disease Unit, Eye Repair Lab, IRCCS San Raffaele Scientific Institute, Milan, Italy
[2]Institute of Experimental Neurology (INSPE), Division of Neuroscience, San Raffaele Scientific Institute, Milan, Italy

Correspondence: Giulio Ferrari, Cornea and Ocular Surface Unit, Eye Repair Lab, IRCCS San Raffaele Scientific Institute, Via Olgettina 60, 20132 Milan, Italy; ferrari.giulio@hsr.it.

Received: May 24, 2021
Accepted: October 4, 2021
Published: October 26, 2021

Citation: Lasagni Vitar RM, Fonteyne P, Chaabane L, Rama P, Ferrari G. A hypothalamic-controlled neural reflex promotes corneal inflammation. *Invest Ophthalmol Vis Sci.* 2021;62(13):21. https://doi.org/10.1167/iovs.62.13.21

Purpose. To test whether an acute corneal injury activates a proinflammatory reflex, involving corneal sensory nerves expressing substance P (SP), the hypothalamus, and the sympathetic nervous system.

Methods. C57BL6/N (wild-type [WT]) and SP-depleted B6.Cg-Tac1tm1Bbm/J (TAC1-KO) mice underwent bilateral corneal alkali burn. One group of WT mice received oxybuprocaine before alkali burn. One hour later, hypothalamic neuronal activity was assessed in vivo by magnetic resonance imaging and ex vivo by cFOS staining. Some animals were followed up for 14 days to evaluate corneal transparency and inflammation. Tyrosine hydroxylase (TH), neurokinin 1 receptor (NK1R), and neuronal nitric oxide synthase (nNOS) expression was assessed in brain sections. Sympathetic neuron activation was evaluated in the superior cervical ganglion (SCG). $CD45^+$ leukocytes were quantified in whole-mounted corneas. Noradrenaline (NA) was evaluated in the cornea and bone marrow.

Results. Alkali burn acutely induced neuronal activation in the trigeminal ganglion, paraventricular hypothalamus, and lateral hypothalamic area (PVH and LHA), which was significantly lower in TAC1-KO mice ($P < 0.05$). Oxybuprocaine application similarly reduced neuronal activation ($P < 0.05$). TAC1-KO mice showed a reduced number of $cFOS^+/NK1R^+/TH^+$ presympathetic neurons ($P < 0.05$) paralleled by higher nNOS expression ($P < 0.05$) in both PVH and LHA. A decrease in activated sympathetic neurons in the SCG and NA levels in both cornea/bone marrow and reduced corneal leukocyte infiltration ($P < 0.05$) in TAC1-KO mice were found. Finally, 14 days after injury, TAC1-KO mice showed reduced corneal opacity and inflammation ($P < 0.05$).

Conclusions. Our findings suggest that stimulation of corneal sensory nerves containing SP activates presympathetic neurons located in the PVH and LHA, leading to sympathetic activation, peripheral release of NA, and corneal inflammation.

Keywords: acute corneal injury, corneal nerves, substance P, hypothalamus, sympathetic nervous system

Eye wounds are the most common cause of injury seen in emergency departments.[1,2] Of these, corneal injuries caused by foreign bodies or superficial abrasion represent approximately 75%, indicating that the corneal epithelium is the most common primary site of injury.[3] Moreover, epithelial injury represents a major cause of visual impairment worldwide, leaving 1.6 million people blind and more than 20 million with unilateral blindness or low vision.[4] Because corneal nerves are most abundant in the epithelium layer, they are among the first structures damaged by ocular trauma. In addition, corneal nerves are altered in the course of highly prevalent ocular surface diseases (e.g., dry eye) or disrupted during refractive surgery procedures.[5,6]

While it is known that nerve damage is associated with pain[7] and can modulate wound healing locally,[8,9] it is unknown whether it acutely affects the functioning of higher brain centers and how this can influence the local and systemic inflammatory response. In a previous study, we demonstrated the existence of a corneal-trigeminal axis, where substance P (SP) promotes the propagation of inflammation from the cornea to the trigeminal ganglion (TG) through corneal nerves.[10] However, involvement of higher brain centers after an acute corneal injury was not investigated.

Interestingly, it has been reported that neurons located in the TG can directly project to the hypothalamus, an area of the brain, which activates the sympathetic nervous system (SNS). Trigemino-hypothalamic fibers convey sensory information from the cornea[11]; therefore, many hypothalamic areas contain trigeminal axons.[12] Among these, the rostral hypothalamus integrates the afferent-sensory information and the efferent-autonomic response[13]; however, its functional relevance in ocular injury and its implications for corneal inflammation remain elusive. In particular, the paraventricular hypothalamus (PVH) and the lateral hypothalamic area (LHA) control vital functions such as

pain and heart rate.[14,15] The regulation of these processes involves the activation of presympathetic neurons located in the PVH and LHA,[16–18] which, in turn, can trigger SNS activity.[19] Recently, the role of SNS in modulating the inflammatory cell influx that occurs hours after a corneal wound has emerged.[20] Yet, the central mechanism controlling the rapid SNS activation occurring after corneal injury needs further elucidation.

In the present work, we hypothesize that after acute corneal injury, corneal sensory nerves projecting to the hypothalamus activate the PVH and LHA, which then trigger an efferent response mediated by the SNS in the cornea and the bone marrow. Furthermore, we hypothesize that SP and its neurokinin 1 receptor (NK1R), which are highly expressed in corneal nerves, mediate hypothalamic activation. To test this hypothesis, we quantified the activation of the specific hypothalamic areas in vivo with functional magnetic resonance imaging (MRI) and ex vivo with immunostainings. Furthermore, we confirmed activation of the SNS by evaluating noradrenaline release in the cornea and the bone marrow.

Materials and Methods

Animals

Eight-week-old male mice C57BL6/N (Charles River, Calco, Italy) (wild-type [WT] mice, total $N = 64$) and Tac1-deficient B6.Cg-Tac1tm1Bbm/J (Jackson Laboratories, Bar Harbor, ME, USA) (TAC1-KO mice, total $N = 48$) were used. Animals were anesthetized with an intraperitoneal injection of tribromoethanol (250 mg/kg) before the surgical procedure. To euthanize the mice, carbon dioxide inhalation followed by cervical dislocation was employed. All experimental protocols were approved by the Animal Care and Use Committee of the San Raffaele Scientific Institute, in accordance with the ARVO Statement for the Use of Animals in Ophthalmic and Vision Research.

Alkali Burn

Corneal alkali burn was created bilaterally in the animals as previously described.[21] Briefly, a paper disc (3 mm diameter) soaked in 1 N NaOH was applied for 10 seconds under slit-lamp examination. Then, the cornea was washed with 15 mL normal saline solution. After 1 hour, in vivo MRI experiments were performed or animals were euthanized to perform immunohistochemical analysis described below.

Another group of WT ($n = 7$) and TAC1-KO ($n = 5$) animals was followed up for 14 days. In vivo corneal photographs were taken using a digital camera (EOS 30D; Canon, Tokyo, Japan) attached to a slit-lamp microscope (Photoslitmap 40 SL-P; Zeiss, Oberkochen, Germany) to assess the corneal condition. Corneal opacity was evaluated using a grading score (from 0 to 5; 0 = completely clear, 4 = completely opaque, 5 = perforation) previously described.[22] On day 14, mice were euthanized and corneas were dissected in order to perform immunofluorescence analysis as described below.

In Vivo Functional Imaging by Manganese-Enhanced MRI

The function of the hypothalamus and trigeminal ganglion was assessed in vivo by manganese-enhanced MRI (MEMRI) in WT ($n = 4$) and TAC1-KO ($n = 4$) mice 1 hour after alkali burn. A constant infusion of manganese (II) chloride ($MnCl_2$) (Sigma-Aldrich, St Louis, MO, USA) through a catheter placed in the tail vein of the mouse was performed to reach the adequate Mn^{2+} concentration. All experiments were performed on a 7-Tesla MRI scanner (BioSpec; Bruker BioSpin Gmbh, Ettlingen, Germany) fully equipped for in vivo imaging in mice. Animals were anesthetized with a mixture of oxygen/isoflurane (97/3% for induction and 98–99/2–1% for maintenance) and placed on a warmed bed to keep the body temperature at 37°C. The breath rate was constantly monitored to adjust the level of anesthesia during the entire MRI examination. For high-resolution MRI, a mouse brain surface array coil was placed over the animal's head. Several T2-weighted (T2w) images were initially acquired in different plans for anatomic reference. Serial acquisitions of T1-weighted (T1w) images were done at baseline (four repetitions) and during manganese infusion (0.2 mL/h, 47 mg/kg) for up to 1 hour.

A spin-echo T1w sequence was used to acquire 14 axial sections across the mouse brain (field of view 14.5 × 9 mm, 172 × 96 matrix size, 0.8-mm slice thickness, 84 × 94 μm^2 in-plane resolution) with a repetition time of 480 ms, echo time of 16 ms, and eight averages, resulting in a total acquisition time of 4 minutes, 37 seconds for each scan. With identical geometry, T2w axial images were acquired with a repetition time of 3000 ms, echo time of 48 ms, and eight averages as the anatomic reference. To quantify manganese (Mn^{2+}) accumulation over the brain, hypothalamic areas (PVH and LHA), TG, and the third ventricle were defined on each T2w image based on the ALLEN mouse brain reference atlas (http://mouse.brain-map.org/static/atlas). The signal intensity of each region of interest was extracted using the scanner software (Paravision 6; Bruker-Biospin Gmbh). The signal intensity was divided by the standard deviation of the noise measured in the image background. Compared to preinfusion scan, signal intensity changes (% enhancement) of each T1w scan acquired during Mn^{2+} infusion were calculated and normalized to the signal from the third ventricle (3V) to limit any variations related to injection dose. Differences of signal-to-noise ratio (SNR) between post- and premanganese administration were calculated as follows for each acquired image over time (t): Enh(t) = 100 * [SNR(t) – SNR(pre)]/SNR(pre).

They were normalized to ventricle signal enhancement as follows: Enh-norm = Enh / [V/<V>], in which V is the signal enhancement measured in the 3V and <V> is the mean value over all animals at the plateau, 40 minutes after manganese administration.

Immunohistochemical Analysis in the Brain

Immunohistochemical analysis was performed in WT ($n = 8$) and TAC1-KO ($n = 8$) mice subjected to bilateral alkali burn. In a group of WT mice ($n = 3$), a 10-µL drop of oxybuprocaine (4 mg/mL), a well-recognized local anesthetic, was applied before alkali burn. After 1 hour, mice were sacrificed. Brains were carefully removed by cutting the skullcap with scissors and lifting with forceps. Then, the brains were washed in cold PBS to remove the excess of blood. Fixation was immediately performed using 4% paraformaldehyde overnight at room temperature (RT) followed by a treatment with 30% sucrose for 2 days at 4°C. Then, they were carefully embedded in the same orientation in optimal cutting temperature medium (OCT Killik;

Investigative Ophthalmology & Visual Science

Bio-Optica, Milan, Italy), and 8-µm cryosections were performed. To identify the PVH or LHA regions, the ALLEN mouse brain reference atlas was used.

Brain sections were postfixed in acetone for 15 minutes on ice and then blocked with 2% bovine serum albumin, 0.1% Triton X-100 (Sigma-Aldrich), and 10% normal donkey serum for 1 hour at RT. The triple immunostaining was performed using chicken anti–tyrosine hydroxylase (TH) (1/800, AB76442; Abcam, Cambridge, UK), rabbit anti-cFOS (cFOS) (1/50, SC52; Santa Cruz Biotechnology, Dallas, Texas, USA), and goat anti-NK1R (1/800, AB61705; Abcam). Other sections were stained with rabbit anti–neuronal nitric oxide synthase (nNOS) (1/200, 4231; Cell Signalling, Danvers, Massachusetts, USA). Secondary detection was performed using Alexa Fluor 594 donkey anti-rabbit IgG (1/1000, A21207; Life Technologies, Carlsbad, California, USA), FITC donkey anti-chicken (1/1000, 703-095-155; Jackson ImmunoResearch, Ely, Cambridgeshire, UK), Alexa Fluor 633 donkey anti-goat (1/1000, A11073; Life Technologies), or Alexa Fluor 488 donkey anti-rabbit IgG (1/1000, A21207; Life Technologies) for 1 hour at RT, diluted in blocking solution. Samples were counterstained with 4,6-diamidino-2-phenylindole (DAPI; Vector Laboratories, Inc., Burlingame, CA, USA) and mounted. Pictures were acquired with a DeltaVision Ultra microscope (GE Healthcare, Chicago, IL, USA) (20×). The image analysis was performed using ImageJ software (National Institutes of Health, Bethesda, MD, USA). A negative control using only the secondary antibody was used to establish a fluorescence threshold in each channel. In addition, isotypes control were performed (Supplementary Material). Then, triple-positive cells (TH^+, $cFOS^+$, $NK1R^+$) were quantified and normalized by the total number of TH^+ cells. The result was expressed as triple-positive cell percentage. $cFOS^+$ or $nNOS^+$ neurons were quantified separately and the results expressed as $nNOS^+$ or $cFOS^+$ cells/section. For the PVH, 10 brain sections and two fields/section were quantified; for the LHA, 20 brain sections and six fields/section were analyzed.

Immunohistochemical Analysis of the Superior Cervical Ganglion

The superior cervical ganglion (SCG) was carefully isolated from WT ($n = 4$) and TAC1-KO ($n = 4$) mice 90 minutes after alkali burn. Briefly, after an incision was made on the ventral neck region, the salivary glands were retracted to expose the underlying muscles. Then, the omohyoid muscles and the common carotid artery were dissected. The SCG was identified behind the carotid bifurcations and gently pulled out.[20] Finally, the SCG was carefully embedded in the same orientation in optimal cutting temperature medium (OCT Killik; Bio-Optica, Milan, Italy), and 8-µm cryosections were performed. The sections were fixed in acetone for 15 minutes on ice and then blocked with 2% bovine serum albumin, 5% normal donkey serum, and 5% normal goat serum for 1 hour at RT. The immunostaining was performed using chicken anti-TH (1/800, AB76442; Abcam) and rabbit anti-cFOS (cFOS) (1/50, SC52; Santa Cruz Biotechnology). Secondary detection was performed using Alexa Fluor 594 donkey anti-rabbit IgG (1/1000, A21207; Life Technologies) and Alexa Fluor 488 goat anti-chicken (1/1000, A11039; Life Technologies) for 1 hour at RT, diluted in blocking solution. Samples were counterstained with DAPI (Vector Laboratories, Inc.) and mounted. A negative control using only the secondary antibody was used to establish a fluorescence threshold in each channel. In addition, isotype control was performed (Supplementary Material). Images were acquired in an epifluorescence microscope (Leica CTR5500; Leica Microsystems, Wetzlar, Germany). ImageJ software (National Institutes of Health) was used to conduct the image analysis. Double-positive cells (TH^+, $cFOS^+$) were quantified and normalized by the total number of TH^+ cells. The result was expressed as double-positive cell percentage.

Noradrenaline Measurement

The concentration of noradrenaline (NA) was determined in cornea and bone marrow samples of WT ($n = 3$) and TAC1-KO ($n = 4$). Alkali burn was generated in the right eye using 1 N NaOH as described before. After 15 or 90 minutes, injured corneas and bone marrow were isolated as previously described.[23,24] Briefly, the cornea was dissected using a sterile scalpel. For the bone marrow isolation, the femur and tibia bones were removed immediately. Bone marrow was obtained by centrifugation at 10,000 × g for 15 seconds. Corneas or bone marrow were homogenized in 150 µL RIPA buffer containing 1% protease inhibitor with Ultra-Turrax T8 (IKA, Wilmington, NC, USA) and then centrifuged at 10,000 rpm for 5 minutes at 4°C. The protein content of the supernatants was quantified with the Bradford protein assay (Thermo Scientific, Waltham, MA, USA). A highly sensitive enzyme-linked immunosorbent assay kit (Product ID: HEA907Ge; Cloud Clone, Wuhan, China) was used, following the manufacturer's instruction. NA levels were expressed as pg/mg protein.

Leukocyte Infiltration Analysis

Mice were subjected to bilateral 5 M NaCl stimulus as described before[25] to specifically stimulate corneal nerves. A drop (10 µL) of PBS (WT: $n = 7$ and TAC1-KO: $n = 11$), fosaprepitant (10 mg/mL in PBS, $n = 13$), or timolol (5 mg/mL; Thea, Keele, Newcastle-under-Lyme, UK) (WT: $n = 10$ and TAC1-KO: $n = 8$) was topically applied for 1 minute. Three minutes after the treatment, the eyes were stimulated with 5 M NaCl. The procedure was repeated four times in 1-hour intervals. One hour after the last stimulus, mice were euthanized and corneas were dissected and stained with goat anti-CD45 (1/200, AF-114; R&D Systems, Minneapolis, MN, USA). Secondary detection was performed using Alexa Fluor 633 donkey anti-goat (1/1000, A11073; Life Technologies). Immune cell infiltration was quantified in the whole mounts by counting the $CD45^+$ cells per field (six peripheral and three central fields; 20×, 5 µm, z-stack). Then, an average was performed, and this number was normalized by the field area (0.387 mm^2). Images were acquired with a DeltaVision Ultra microscope (GE Healthcare), and the analysis was performed using ImageJ software (National Institutes of Health). Results were expressed as $CD45^+$ cells/mm^2.

For the alkali burn model, at day 14, WT ($n = 5$) and TAC1-KO ($n = 4$) mice were euthanized and corneas were dissected and stained as described above. $CD45^+$ cell infiltration was quantified in the whole mounts by counting the $CD45^+$ cells as described above. Pictures were taken using a confocal microscope (Leica TCS SP5, 40×, 5 µm, z-stack; field area: 0.150 mm^2). Results were expressed as $CD45^+$ cells/mm^2.

Investigative Ophthalmology & Visual Science

Statistical Analysis

Statistical calculation was performed using GraphPad Prism 5.0 software (GraphPad Software, La Jolla, CA, USA). Data were expressed as mean ± SEM. The statistical significance of the differences between the two groups was calculated by nonparametric tests: Mann–Whitney test (when comparing two groups) or Kruskal–Wallis test, followed by Dunn post hoc test (when comparing more than two groups). A P value lower than 0.05 was considered statistically significant.

Results

Acute Corneal Injury Induces Activation of the Trigeminal Ganglion and Specific Hypothalamic Areas

WT and TAC1-KO mice underwent alkali burn bilaterally to test after 1 hour the neuronal activity in the TG and in the hypothalamus. In the hypothalamus, specific regions related to the SNS, the PVH, and the LHA were evaluated (Fig. 1A). Figure 1B displays representative images of the in vivo MRI 1 hour after bilateral corneal alkali burn. As shown, the WT mice presented higher manganese contrast uptake in the three regions of interest, TG, PVH, and LHA, which means a higher neuronal activity. It is well known that the paramagnetic manganese ions (Mn^{2+}) enter synaptically activated neurons through voltage-gated calcium channels, which is observed as signal enhancement on T1w MRI images.[26] Several studies have demonstrated the potential of MEMRI to detect in vivo hypothalamic neuronal activity in various mouse models.[27–29] In the present study, the quantification of the signal enhancement showed that TAC1-KO mice displayed a significant decrease in the TG (507.8% ± 41.7%, P = 0.0286), PVH (330.8% ± 19.8%, P = 0.0286), and LHA (319.5% ± 21.7%, P = 0.0286) compared to WT mice (TG: 775.5% ± 103.1%; PVH: 438.4% ± 24.3%; LHA: 409.1% ± 21.0%) (Fig. 1C). Of note, there was no difference in neuronal density when compared with WT and TAC1-KO mice (Supplementary Fig. S1). These results suggest that after an acute corneal injury, trigeminal neurons as well as specific hypothalamic regions related to the SNS are activated in an SP-dependent manner.

Acute Corneal Injury Induces Activation of TH^+ Neurons Coexpressing NK1R in the PVH and LHA

The triple staining of TH, cFOS, and NK1R showed that activated presympathetic neurons in the PVH and LHA also expressed NK1R (Fig. 2A). When the triple-positive cells (TH^+, $cFOS^+$, $NK1R^+$) were quantified in WT mice, we observed that out of the total TH^+ neurons found in the PVH (6.5 ± 0.4) and LHA (7.1 ± 0.2 cells), 55% (3.3 ± 0.9 cells) and 30% (2.0 ± 0.3 cells), respectively, were activated ($cFOS^+$) and expressed NK1R. TAC1-KO mice showed a similar number of TH^+ cells (PVH: 6.6 ± 2.5; LHA: 8.7 ± 1.6) but a reduced number of the triple-positive neurons in both PVH (17%, 1.2 ± 0.2 cells, P = 0.0477) and LHA (4%, 0.4 ± 0.3 cells, P = 0.0498) (Fig. 2B), confirming the reduced neuronal activity observed in vivo by MRI. Of note, not all the $cFOS^+$ neurons were TH^+, suggesting that other types of neurons were also activated in this experimental setting.

Acute Corneal Injury Decreases Expression of nNOS in the PVH and LHA, Which Is Inhibited by SP Ablation

In Figure 3A, representative immunofluorescence images (20×) of WT and TAC1-KO mice after bilateral corneal alkali burn are displayed. Quantification of nNOS-positive neurons showed an increase of nNOS expression in the PVH and LHA of TAC1-KO mice when compared to WT (P = 0.0159 and P = 0.0159, respectively) (Fig. 3B).

Corneal Sensory Nerve Stimulation Activates Hypothalamic Neurons in the PVH and LHA

Neuronal activation in the PVH and LHA was assessed by cFOS immunostaining in WT, TAC1-KO, WT + local anesthetic, and WT noninjured mice (Fig. 4A). When $cFOS^+$ neurons were quantified, both TAC1-KO and WT + local anesthetic mice showed a lower number of activated neurons compared to WT (P = 0.0286 and P = 0.0075, respectively). Moreover, no significant differences were found among TAC1-KO, WT + local anesthetic, and WT noninjured groups (Fig. 4B). These results suggest that after an acute corneal injury, the sensory nerves containing SP are mainly responsible for the neuronal activation in the PVH and LHA.

Acute Corneal Injury Induces Activation of Sympathetic Neurons in the SCG

cFOS and TH double staining was employed to detect sympathetic neuron activation in the SCG after an acute corneal injury in WT and TAC1-KO mice (Fig. 5A). While TH^+ neurons did not vary between both groups, activated TH^+ $cFOS^+$ neurons were significantly lower in TAC1-KO mice (9.0 ± 4.7 TH^+ $cFOS^+$ cells, P = 0.0286) when compared to WT mice (77.5 ± 14.4 TH^+ $cFOS^+$ cells) (Fig. 5B). These results suggest that sympathetic neurons located in the SCG are activated following acute corneal nerve stimulation.

Sensory Stimulation Results in Increased Noradrenaline Release and Leukocyte Infiltration in the Cornea

In order to evaluate the sympathetic activation in the cornea, we determined the levels of NA after corneal injury. In line with our previous results, TAC1-KO mice displayed lower levels of NA in the cornea after 90 minutes (11.4 ± 2.1 pg/mg, P = 0.0286) when compared to WT mice (28.1 ± 3.3 pg/mg) (Fig. 6A). In addition, we evaluated the NA release in the bone marrow. We found that 15 minutes after alkali burn, NA levels in the bone marrow were lower in TAC1-KO mice (2.7 ± 0.8 pg/mg, P = 0.0500) compared to WT mice (5.6 ± 0.4 pg/mg) (Fig. 6B).

In this context, we quantified the leukocyte infiltration in the cornea. Figure 6C shows representative images (20×) of whole-mount corneas of WT + PBS, WT + fosaprepitant (NK1R antagonist), WT + timolol (β2-blocker), TAC1-KO + PBS, and TAC1-KO + timolol mice after an acute hypertonic saline insult that specifically stimulates corneal nerves. Quantification of $CD45^+$ cells showed a reduced number in WT + fosaprepitant (P = 0.0003), WT + timolol (P = 0.0020), TAC1-KO (P = 0.0006), and TAC1-KO + timolol (P = 0.0006) mice compared to WT. In addition, WT + fosaprepitant mice

Investigative Ophthalmology & Visual Science

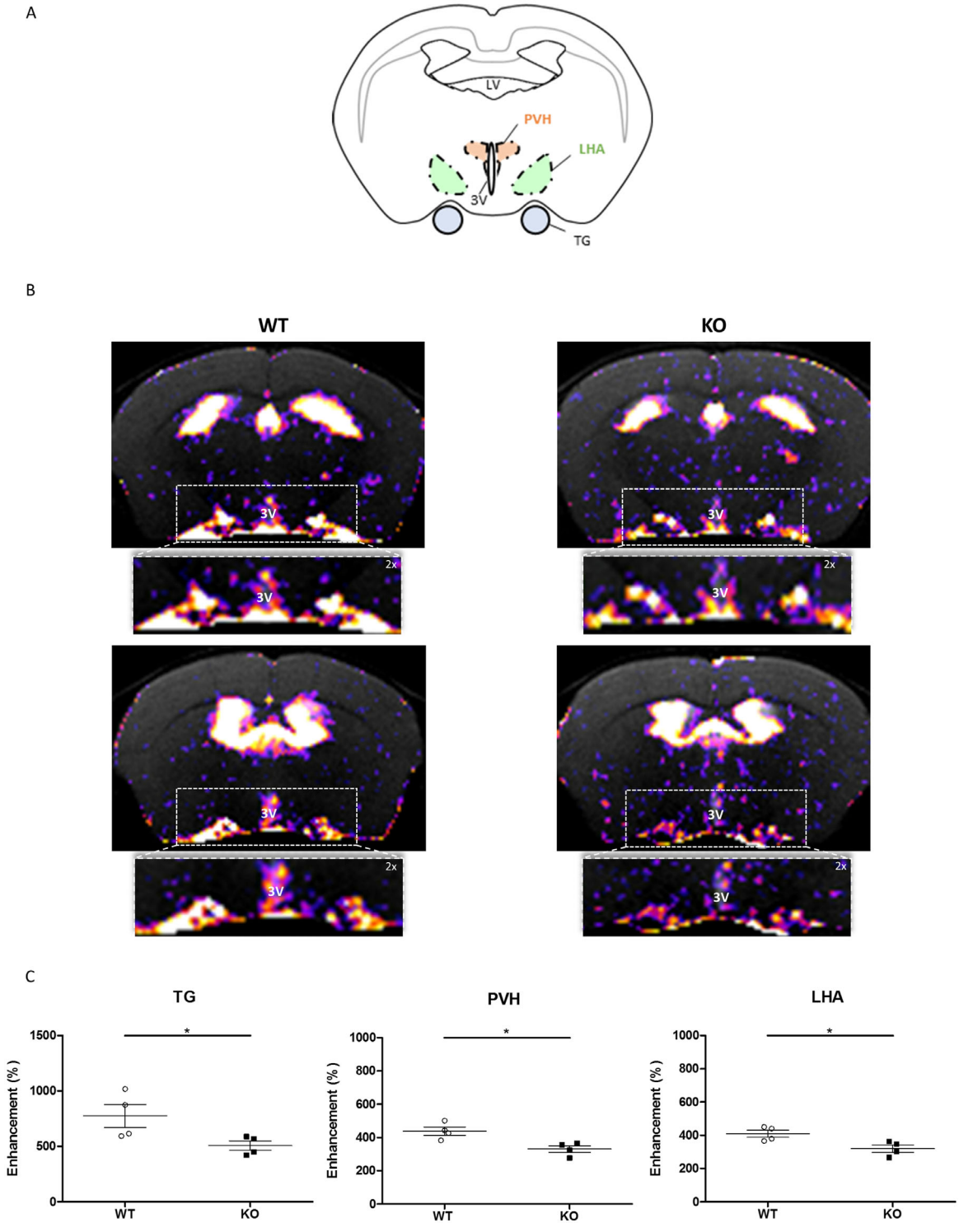

Figure 1. Acute corneal injury induces activation of trigeminal ganglia and specific hypothalamic areas. (**A**) Scheme of a coronal brain section illustrating the hypothalamic regions of interest (PVH and LHA) and the relative position of the TG. (**B**) Representative images of in vivo MRI 1 hour after bilateral corneal alkali burn in WT ($n = 4$) and TAC1-KO ($n = 4$) mice. The images are consecutive coronal sections 0.8 mm thick. (**C**) Quantification of the signal enhancement (%), showing that TAC1-KO mice displayed a significant decrease in tracer uptake in the TG, PVH, and LHA compared to WT mice. Graphs represent mean ± SEM; statistical analysis by Mann–Whitney test. *$P < 0.05$.

showed a significantly lower amount of $CD45^+$ cells than WT + timolol mice ($P = 0.0006$) (Fig. 6D).

Additionally, we quantified the $CD45^+$ cells in the bloodstream after hypertonic saline application on the cornea, which specifically stimulates corneal nerves without severe damage. In a group of mice, we previously applied a local anesthetic to test if the observed systemic increase of leukocytes was a direct consequence of corneal nerve stimulation.

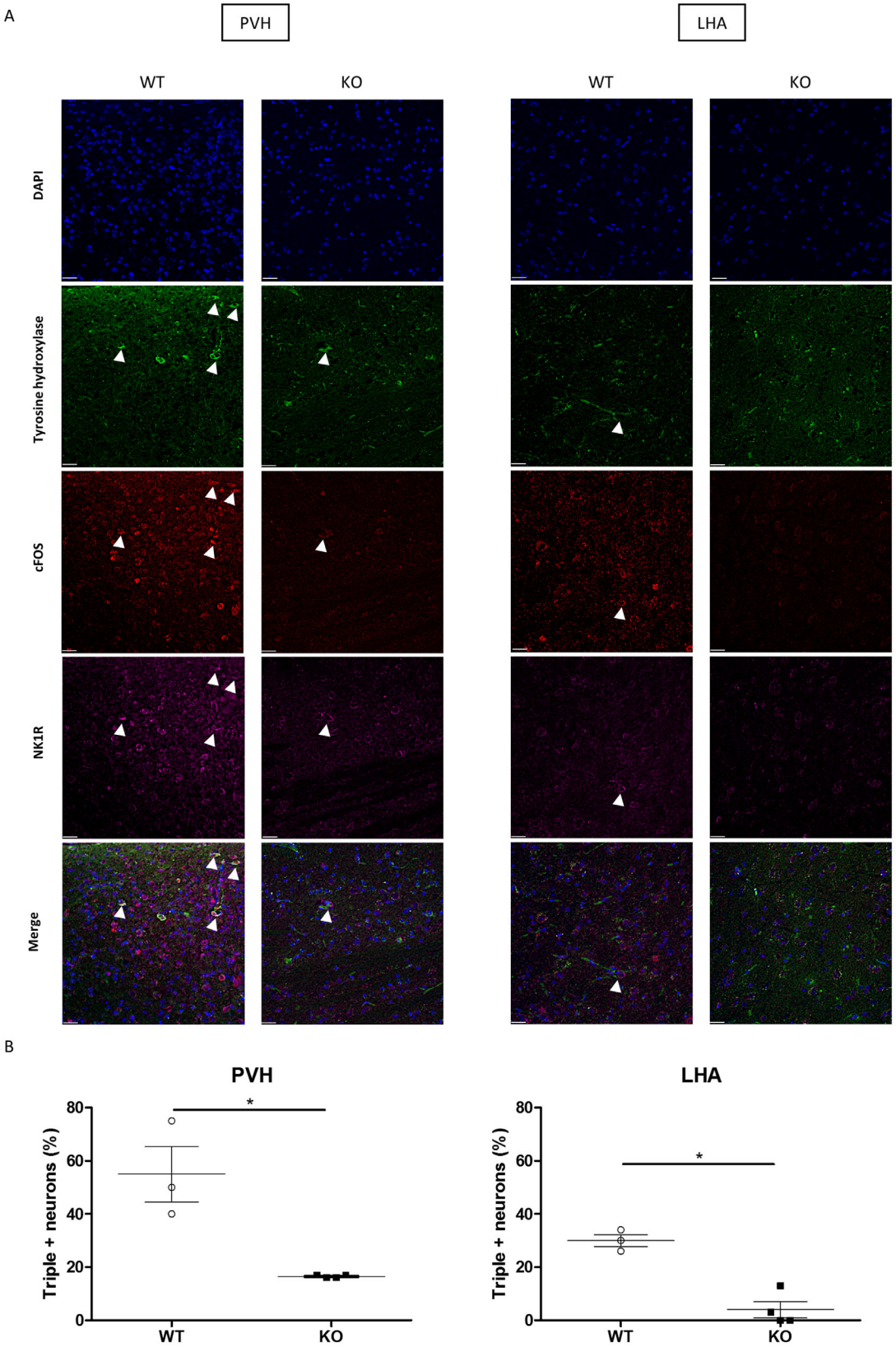

Figure 2. Acute corneal injury induces activation of presympathetic neurons coexpressing NK1R in the PVH and LHA. (**A**) Activated presympathetic neurons (cFOS$^+$ and TH$^+$) that expressed NK1R were assessed by immunofluorescence. Representative images (20×) of WT ($n = 3$) and TAC1-KO ($n = 4$) mice after bilateral corneal alkali burn. Triple-positive neurons are shown with *arrowheads*. (**B**) Quantification of triple-positive neurons expressed as a percentage over the total number of TH$^+$ neurons in the PVH and the LHA. TAC1-KO mice showed a decreased activation of sympathetic neurons coexpressing NK1R. Graphs represent mean ± SEM; statistical analysis by Mann–Whitney test. *$P < 0.05$. *Scale bar*: 25 µm.

Investigative Ophthalmology & Visual Science

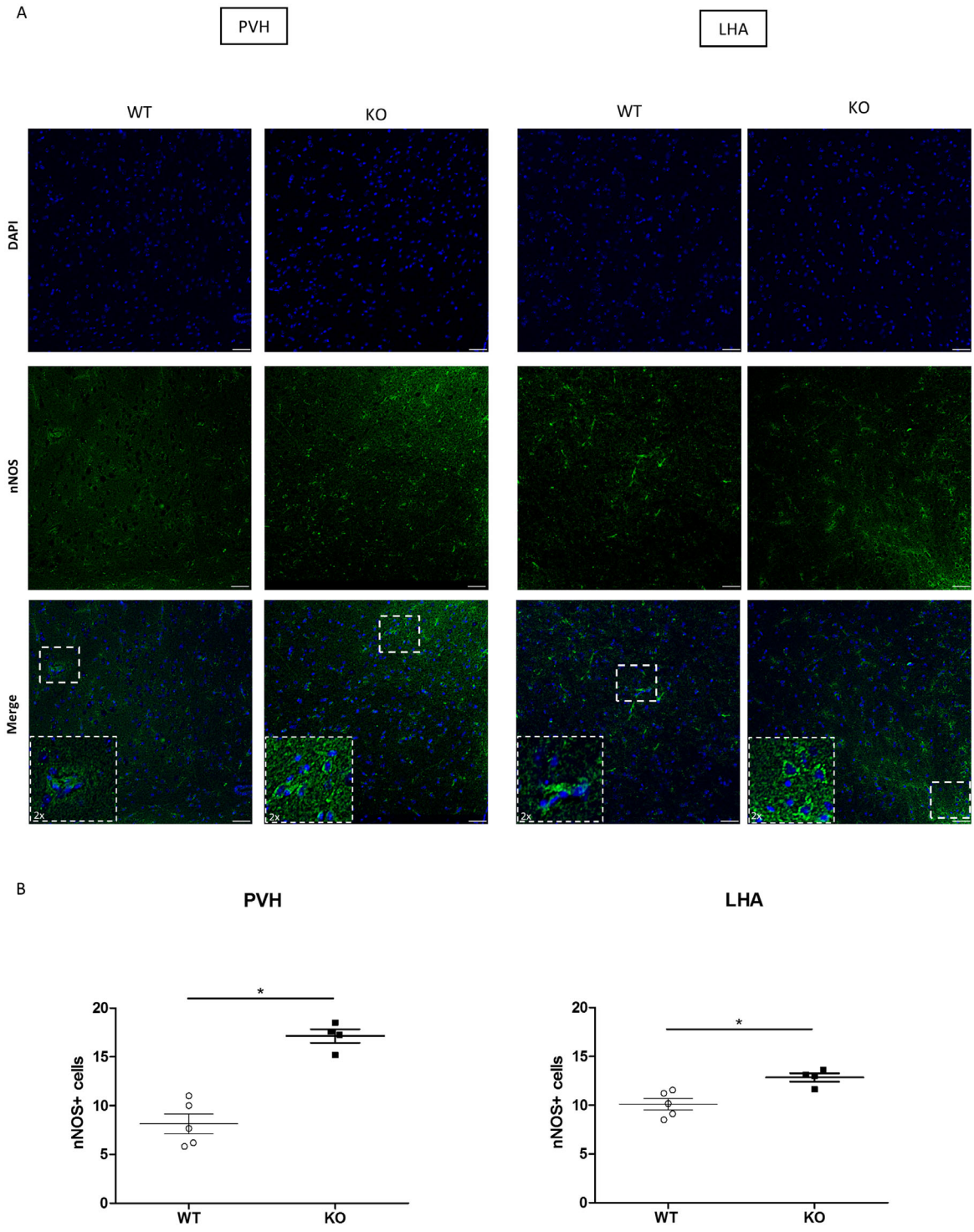

Figure 3. Acute corneal injury promotes a decrease of sympathetic inhibitor nNOS in the PVH and LHA that is counteracted by SP ablation. (**A**) nNOS expression was assessed by immunofluorescence. Representative images (20×) of WT ($n = 5$) and TAC1-KO ($n = 4$) mice after bilateral corneal alkali burn. (**B**) Quantification of $nNOS^+$ neurons. As it is shown, TAC1-KO mice displayed an increase in nNOS expression in the PVH and the LHA after an acute corneal injury. Graphs represent mean ± SEM; statistical analysis by Mann–Whitney test. *$P < 0.05$. *Scale bar*: 25 µm.

We found that when local anesthetics were applied before the stimulus, a reduced level of circulating $CD45^+$ leukocytes was observed ($P = 0.0080$) (Supplementary Fig. S2).

Altogether, these results suggest that as a consequence of corneal sensory nerve stimulation, sympathetic activation through the SP/NK1R pathway leads to increased leukocyte

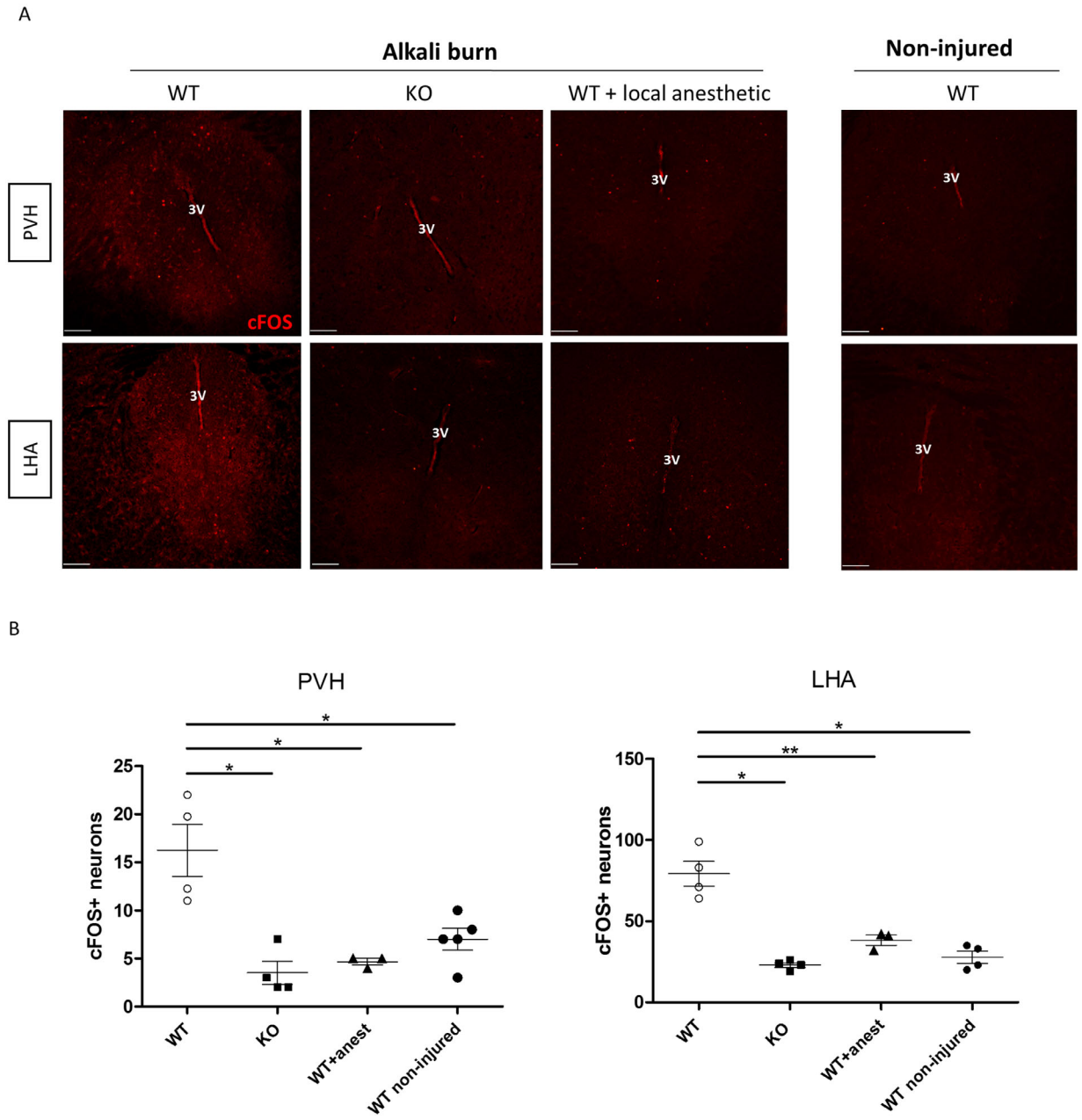

Figure 4. Corneal sensory nerve stimulation activates hypothalamic neurons in the PVH and LHA. (**A**) cFOS immunostaining was employed to detect neuronal activation. Representative immunofluorescence images (10×) of WT ($n = 4$), TAC1-KO ($n = 4$), and WT mice using local anesthetic (4 mg/mL oxybuprocaine) ($n = 3$) after bilateral corneal alkali burn and WT noninjured mice ($n = 5$). (**B**) Quantification of cFOS$^+$ neurons. TAC1-KO mice showed decreased number of activated neurons compared to WT mice, while no significant differences were found when compared to WT with local anesthetics and WT noninjured. Graphs represent mean ± SEM; statistical analysis by Mann–Whitney test or Kruskal–Wallis test, followed by Dunn post hoc test. *$P < 0.05$. **$P < 0.01$. *Scale bar*: 100 µm.

recruitment from the bone marrow and infiltration in the cornea.

SP Ablation Improves Corneal Transparency and Reduces Inflammation After Alkali Burn

Mice that underwent alkali burn were followed up for 14 days to evaluate corneal opacity. As shown in Figure 7A, at day 14 after alkali burn, TAC1-KO mice presented a significant decrease of corneal opacity compared to WT mice ($P = 0.0495$). In addition, a reduced number of CD45$^+$ cells infiltrating the cornea was observed in TAC1-KO mice ($P = 0.0457$) (Fig. 7B). These results suggest that SP ablation improves corneal transparency by reduction of leukocyte infiltration.

Discussion

Increasing evidence suggests that sensory nerves play a central role in the modulation of the corneal inflammatory response.[30,31] Moreover, corneal injury and nerve damage

Investigative Ophthalmology & Visual Science

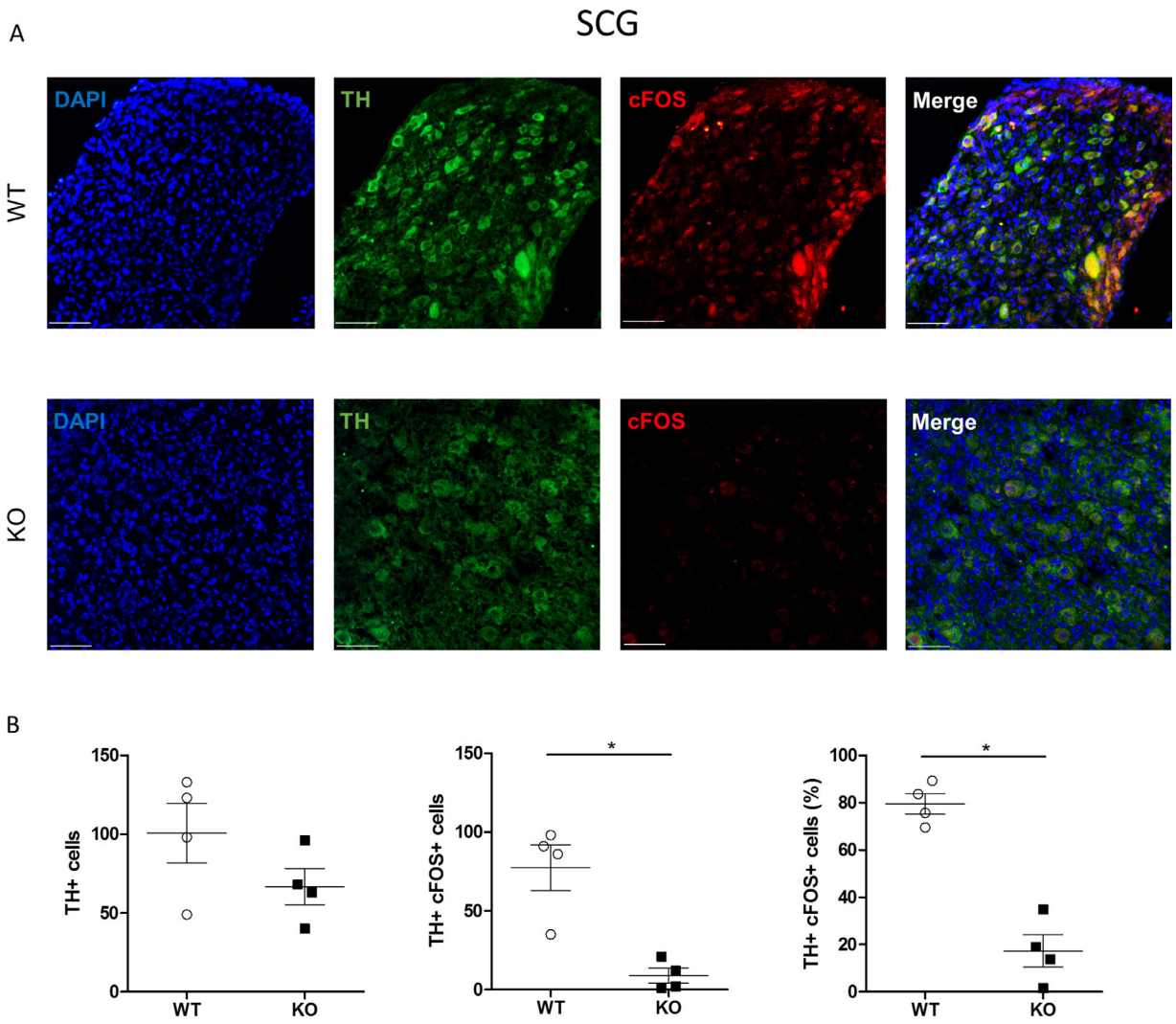

Figure 5. Acute corneal injury stimulates sympathetic neuron located in the superior cervical ganglion, which is inhibited by SP ablation. (**A**) TH and cFOS immunostaining was used to detect neuronal activation in the SCG. Representative immunofluorescence images (20×) of WT ($n = 4$) and TAC1-KO ($n = 4$) mice after bilateral corneal alkali burn. (**B**) Quantification of TH^+ neurons and TH^+ $cFOS^+$ neurons. Graphs represent mean ± SEM; statistical analysis by Mann–Whitney test. *$P < 0.05$. *Scale bar*: 75 µm.

can induce inflammation in the trigeminal ganglion.[10] Similarly, corneal inflammation promotes activation of neural pathways within the trigeminal sensory complex.[32]

The hypothalamus is an area of the brain deeply involved in responses to pain and, more generally, stress.[33,34] Therefore, it is reasonable to hypothesize that corneal injury can affect the functioning of the hypothalamus. The anatomic pathway connecting corneal sensory nerves with the hypothalamus has been mapped[11,12]; however, its functional relevance in corneal inflammation has never been investigated before.

Interestingly, the hypothalamus is the master regulator of the SNS activity[35] because it is the place where presympathetic neurons are located. In fact, two hypothalamic nuclei, LHA and PVH, receive nociceptive inputs from the TG,[36] and their outputs regulate the SNS response to stress and pain.[37] The SNS also modulates the inflammatory response in most tissues, including the cornea, typically by local release of NA.[38]

Here we show, for the first time, that acute corneal injury rapidly activates presympathetic neurons located in the PVH and LHA; this ultimately leads to SNS activation and NA release in the cornea and in the bone marrow (Fig. 8). Moreover, we demonstrate that SP plays a key role in hypothalamus activation, as supported by the observation that SP ablation abolished hypothalamus and SNS activation, ultimately resulting in reduced corneal inflammation and opacity.

It is not surprising that SP plays a key role in this proinflammatory neural reflex since corneal epithelial nerves contain large amounts of SP.[39] Previous work from our group showed that acute corneal injuries induce increased expression of SP and its principal receptor NK1R in both cornea[40] and TG.[10] More recently, it has been reported that sensory neurons directly promote angiogenesis via SP signaling in response to corneal inflammation.[41]

Prior evidence corroborates our finding that the activity of hypothalamic presympathetic neurons is influenced by SP.[42,43] In fact, SP can increase presympathetic neuron

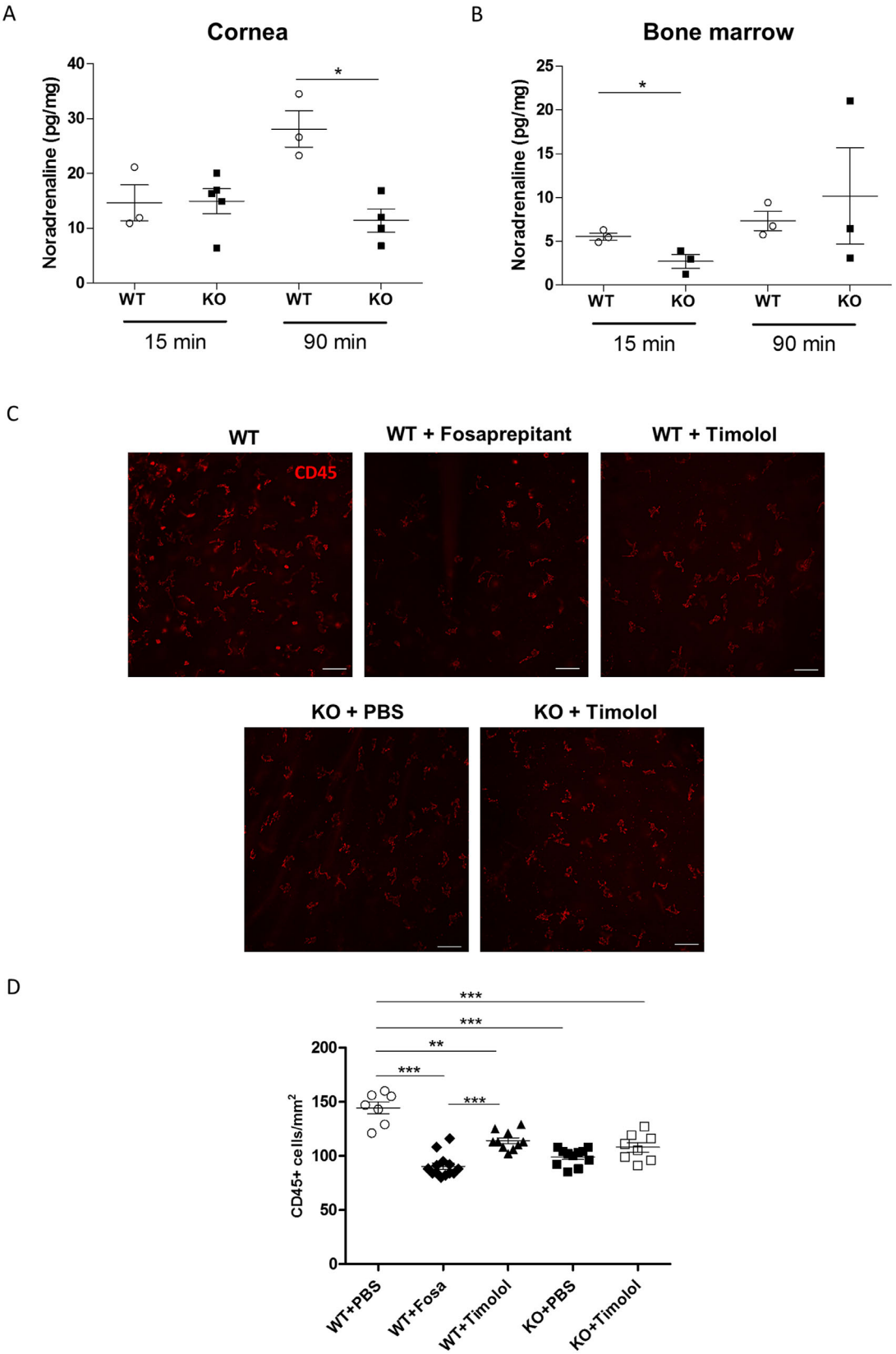

Figure 6. Sensory stimulation results in increased noradrenaline release in the cornea and the bone marrow, as well as corneal leukocyte infiltration. (**A**, **B**) Noradrenaline concentration measured by ELISA in the cornea (WT, $n = 3$; KO, $n = 4$) and the bone marrow (WT, $n = 3$; KO, $n = 3$) after 15 and 90 minutes of bilateral alkali burn. C-leukocyte infiltration was assessed in corneal whole mounts by CD45 immunostaining. Representative immunofluorescence images (20×) of WT + PBS ($n = 7$), WT + fosaprepitant ($n = 13$), WT + timolol ($n = 10$), TAC1-KO + PBS ($n = 11$), and TAC1-KO + timolol ($n = 8$) mice after corneal sensory nerve stimulation with hypertonic saline. (**D**) $CD45^+$ cells were quantified as cells/mm^2. Graphs represent mean ± SEM; statistical analysis by Mann–Whitney test or Kruskal–Wallis test, followed by Dunn post hoc test. *$P < 0.05$. **$P < 0.01$. *Scale bar*: 25 µm.

Investigative Ophthalmology & Visual Science

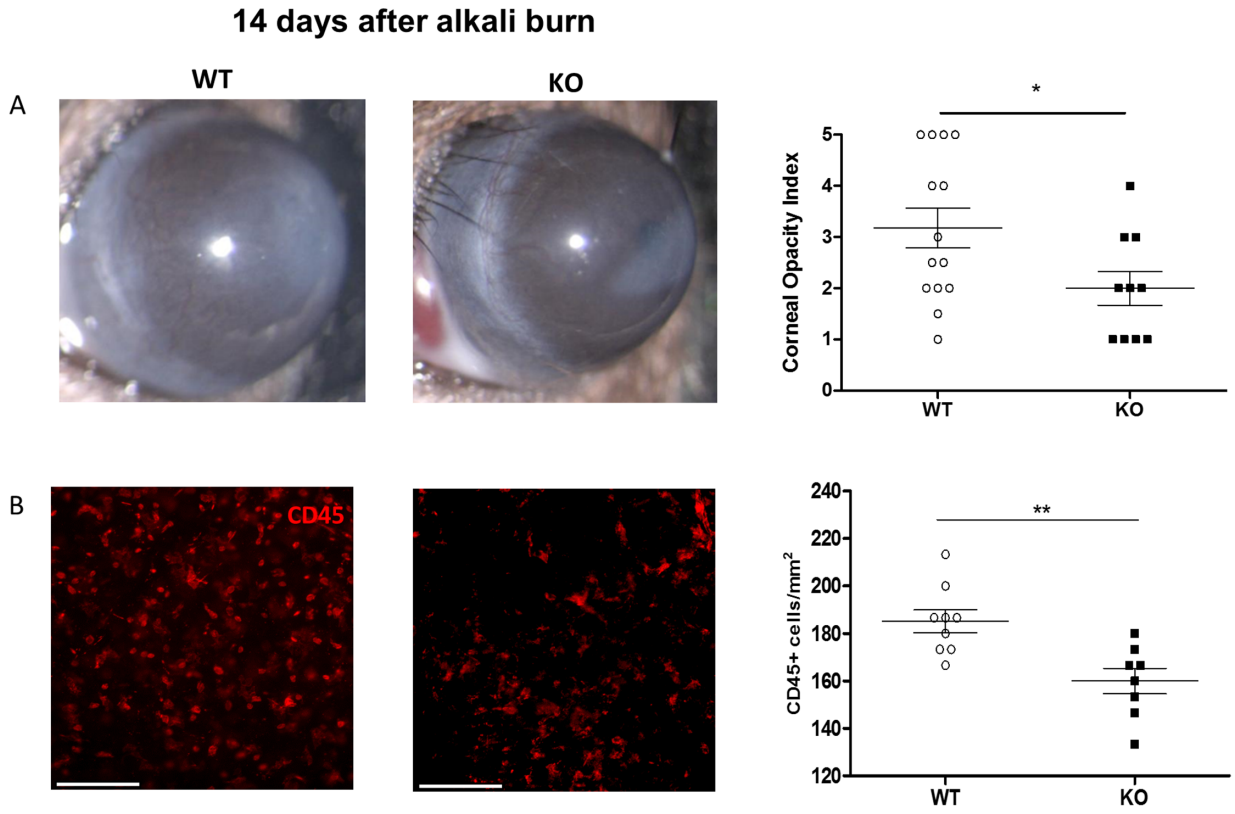

Figure 7. SP ablation results in reduced corneal opacity and inflammation after alkali burn. (**A**) In vivo evaluation of corneal opacity in WT and TAC1-KO mice. Representative slit-lamp pictures of alkali burn eyes after 14 days (WT, $n = 14$ eyes; KO, $n = 10$ eyes). Corneal opacity index was calculated using a grading score (from 0 to 5; 0 = completely clear, 4 = completely opaque; 5 = perforation). TAC1-KO mice showed less corneal opacity after 14 days. (**B**) Representative immunofluorescence images (20×) of WT ($n = 9$ eyes) and TAC1-KO ($n = 8$ eyes) mice 14 days after alkali burn. Quantification of $CD45^+$ leukocytes as cells/mm^2. Graphs represent mean ± SEM; statistical analysis by Mann–Whitney test. $^{**}P < 0.01$. $^{***}P < 0.001$. *Scale bar*: 100 µm.

excitability through inhibition of GABA currents.[44] In addition, inhibition of sympathetic activity by GABA is nitric oxide dependent,[42] which means that an increase in nitric oxide production promotes sympathetic inhibition. In line with these results, we showed that SP ablation increases the expression of nNOS, which can explain the lower hypothalamic activation observed in SP-KO mice. Furthermore, our data show that hypothalamic presympathetic neurons express NK1R, which suggests that SP can directly and locally regulate their activation. Indeed, others have previously shown that activation of the SP/NK1R pathway increases the excitability of spinally projecting neurons in the PVH.[44,45] It is the first time, however, that SP-dependent activation of the hypothalamus has been demonstrated after acute corneal injury.

Altogether, our results support the existence of a neural reflex constituted by an afferent branch (i.e., corneal nerves), an efferent branch (i.e., SNS), and a central regulator (i.e., hypothalamus). SP and its NK1 receptor have a key role in the generation of this reflex.

Activation of the SNS is confirmed by our observation of increased activation of sympathetic neurons located in the SCG that ultimately induces NA release in the cornea, which is accompanied by leukocyte infiltration (Fig. 8). Since corneal NA derives mostly from nerves,[46,47] we conclude that NA secretion is a direct consequence of SNS activation.

We also show that the blockade of the sensory afferent branch abolishes the secondary SNS response. We acknowledge that SNS activation could also be induced by concomitant factors (e.g., stress); however, topical application of a local anesthetic inhibited hypothalamic activation, suggesting that corneal nerves are largely responsible for this phenomenon.

Moreover, we demonstrate that hypothalamic activation after corneal injury is SP dependent by using a transgenic mouse model where SP is ablated. We cannot exclude that the inhibition of neuronal activation is also a consequence of SP ablation in the brain. However, we have recently reported that NK1R blockade in the cornea of WT mice prevents release of SP in the TG, effectively reducing corneal pain and inflammation.[25] The fact that hypothalamus-projecting neurons, which also innervate the cornea, are located in the TG[11] strongly suggests that SP^+ corneal nerves are responsible for hypothalamus activation. We acknowledge that other indirect neuronal pathways involving second-order neurons could be at play as well, contributing to the hypothalamic activation. In any case, SP/NK1R pathway activation represents a key regulator of hypothalamic stimulation.

In support of our findings, other nerve reflexes controlling the inflammatory response have been described before. For instance, an anti-inflammatory nerve reflex has been described in the liver, heart, spleen, and gastrointestinal system.[48] Such a reflex consists of an afferent sensory nerve branch, activated by cytokines or pathogen-derived products, and an efferent, parasympathetic-mediated branch, which acts through release of acetylcholine.[49]

Investigative Ophthalmology & Visual Science

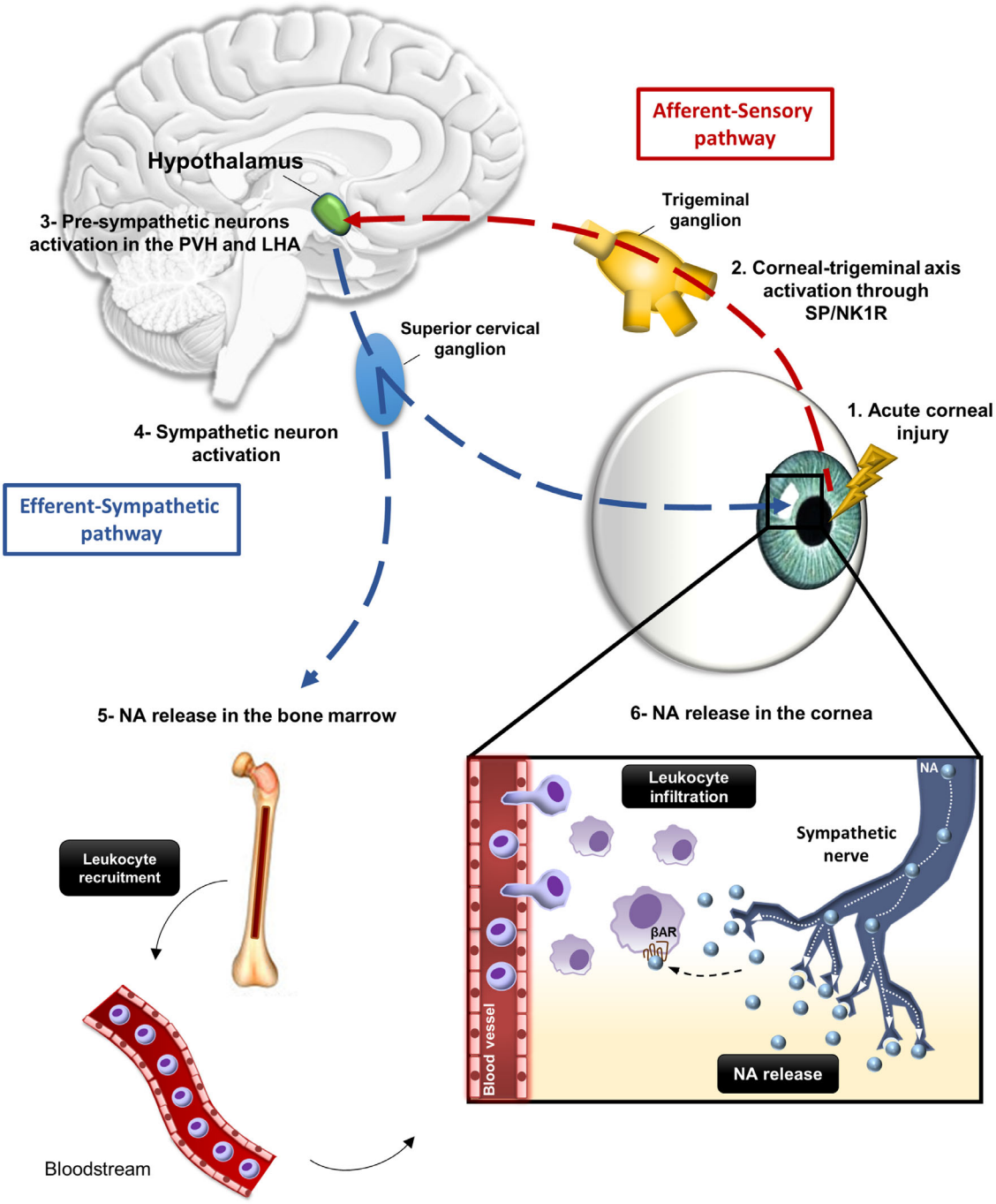

Figure 8. Brain-controlled neural reflex. After acute corneal injury, the afferent branch consisting of sensory nerves containing SP rapidly activates presympathetic neurons in the PVH and the LHA, which coordinate the sympathetic-efferent response. As a consequence, sympathetic neurons are activated in the SCG, and an increased release of NA in the bone marrow and the cornea is observed, accompanied by an increase in circulating leukocytes and corneal leukocyte infiltration.

The role of SNS in corneal inflammation has been studied before, and it is generally thought it is mediated by noradrenaline.[46,47] Specifically, it is known that after corneal injury, the SNS promotes leukocyte recruitment and inflammation. This has clinical implications, because it results in delayed wound healing,[20] promotion of pain through sensitization of sensory terminals,[50] and persistent inflammation in infectious keratitis.[51] Here, we demonstrated that SNS activation acutely promotes corneal inflammation, which was inhibited when a β-blocker was topically applied. Interestingly, local application of the NK1R antagonist fosaprepitant induced a stronger inhibition of leukocyte infiltration. This could be explained based on the premise that NK1R is also present in sensory nerve terminals in the cornea, and therefore, its blockade can inhibit the afferent pathway,[25] in addition to the inhibitory effect on inflammatory cells. On the

other hand, a positive loop between NA and SP has been previously described, in which NA promotes SP release by binding to α-adrenoceptor.[50,52,53] In this vein, it is reasonable to hypothesize that despite blocking the β-receptors located on inflammatory cells, NA can still favor SP release through α-adrenoceptor. Therefore, blocking NK1R would inhibit the inflammatory response by preventing SP effects on both the afferent and efferent pathways. In this context, it is probable that the outcomes we observed in the TAC1-KO mice after acute corneal injury result from a combination of reduced hypothalamic activation and the absence of SP in the cornea. Moreover, when we applied timolol to the TAC1-KO mice, no differences were observed between TAC1-KO + PBS and TAC1-KO + timolol, supporting the reduced hypothalamic activity and, as a consequence, the decreased SNS activation.

Interestingly, we observed that the effects of SNS activation are not restricted to the cornea, since we observed a rapid release of NA in the bone marrow and also a prompt increase in the number of circulating leukocytes. Of note, to evaluate the systemic release of NA, we decided to use the bone marrow because it mainly originates from sympathetic innervation,[54] unlike the plasma that largely contains NA released from the adrenal gland. Our observation that corneal nerve anesthesia prevents leukocytosis further corroborates their relevance in the proinflammatory reflex. In line with our results, it has been previously reported that stimulation of PVH increases the sympathetic tone in the bone marrow, promoting a systemic inflammatory response[55] through different mechanisms involving NA receptors expressed on various populations of bone marrow cells.[20] Interestingly, SP ablation inhibited SNS activation (lower activation of sympathetic neurons in the SCG and lower levels of NA in both cornea and bone marrow), reducing corneal inflammation and, ultimately, improving corneal transparency.

In summary, our work demonstrates the existence of a sensory-sympathetic reflex orchestrated by the hypothalamus and mediated by SP, which promotes inflammation locally and systemically. This mechanism has manifold implications for corneal diseases in terms of clinical translation. First, it supports the rationale of inhibiting SP and/or NA to control corneal inflammation. Pharmacologic blockade of NA (e.g., β-blockers) or SP (e.g., NK1R antagonists) are available and can be exploited for ocular use. Second, they suggest that modulation of hypothalamic activity (and, specifically, of the PVH and LHA) can control inflammation in peripheral organs (i.e., the cornea). Further experiments are needed to evaluate the acute participation of additional central structures such as the trigeminal nucleus and second-order neurons in this complex pathway.

Acknowledgments

The authors thank the Center of Experimental Imaging for support for all in vivo MRI experiments and the Advanced Light and Electron Microscopy BioImaging Center (ALEMBIC) at the IRCCS San Raffaele Hospital for helpful assistance in the immunofluorescence experiments.

Supported by institutional funding.

Disclosure: **R.M. Lasagni Vitar**, None; **P. Fonteyne**, None; **L. Chaabane**, None; **P. Rama**, P; **G. Ferrari**, P

References

1. Négrel A, Thylefors B. The global impact of eye injuries. *Ophthalmic Epidemiol*. 1998;5(3):143–169.
2. Whitcher JP, Srinivasan M, Upadhyay MP. Corneal blindness: a global perspective. *Bull World Health Organ*. 2001;79(3):214–221.
3. McGwin G, Owsley C. Incidence of emergency department-treated eye injury in the United States. *Arch Ophthalmol*. 2005;123(5):662–666.
4. Pascolini D, Mariotti SP. Global estimates of visual impairment: 2010. *Br J Ophthalmol*. 2012;96(5):614–618.
5. Dastjerdi MH, Al-Arfaj KM, Nallasamy N, et al. Topical bevacizumab in the treatment of corneal neovascularization; results of a prospective, open-label, noncomparative study. *Arch Ophthalmol*. 2009;127(4):381–389.
6. Linna TU, Vesaluoma MH, Pérez-Santonja JJ, Petroll WM, Alió JL, Tervo TMT. Effect of myopic LASIK on corneal sensitivity and morphology of subbasal nerves. *Invest Ophthalmol Vis Sci*. 2000;41(2):393–397.
7. McKay TB, Seyed-Razavi Y, Ghezzi CE, et al. Corneal pain and experimental model development. *Prog Retin Eye Res*. 2019;71:88–113.
8. Belmonte C, Acosta MC, Merayo-Lloves J, Gallar J. What causes eye pain? *Curr Ophthalmol Rep*. 2015;3(2):111–121.
9. Słoniecka M, Le Roux S, Boman P, Byström B, Zhou Q, Danielson P. Expression profiles of neuropeptides, neurotransmitters, and their receptors in human keratocytes in vitro and in situ. *PLoS One*. 2015;10(7):e0134157.
10. Ferrari G, Bignami F, Giacomini C, et al. Ocular surface injury induces inflammation in the brain: in vivo and ex vivo evidence of a corneal–trigeminal axis. *Invest Ophthalmol Vis Sci*. 2014;55(10):6289–6300.
11. Malick A, Strassman AM, Burstein R. Trigeminohypothalamic and reticulohypothalamic tract neurons in the upper cervical spinal cord and caudal medulla of the rat. *J Neurophysiol*. 2000;84(4):2078–2112.
12. Malick A, Burstein R. Cells of origin of the trigeminohypothalamic tract in the rat. *J Comp Neurol*. 1998;400(1):125–144.
13. Lumb BM, Lovick TA. The rostral hypothalamus: an area for the integration of autonomic and sensory responsiveness. *J Neurophysiol*. 1993;70(4):1570–1577.
14. Ferguson A V., Latchford KJ, Sanon WK. The paraventricular nucleus of the hypothalamus—a potential target for integrative treatment of autonomic dysfunction. *Expert Opin Ther Targets*. 2008;12(6):717–727.
15. Fakhoury M, Salman I, Najjar W, Merhej G, Lawand N. The lateral hypothalamus: an uncharted territory for processing peripheral neurogenic inflammation. *Front Neurosci*. 2020;14:101.
16. Shi H, Bartness TJ. Neurochemical phenotype of sympathetic nervous system outflow from brain to white fat. *Brain Res Bull*. 2001;54(4):375–385.
17. Shi YC, Lau J, Lin Z, et al. Arcuate NPY controls sympathetic output and BAT function via a relay of tyrosine hydroxylase neurons in the PVN. *Cell Metab*. 2013;17(2):236–248.
18. Janig W. Systemic and specific autonomic reactions in pain: efferent, afferent and endocrine components. *Eur J Anaesthesiol*. 1985;2(4):319–346.
19. Patel KP. Role of paraventricular nucleus in mediating sympathetic outflow in heart failure. *Heart Fail Rev*. 2000;5(1):73–86.
20. Xue Y, He J, Xiao C, et al. The mouse autonomic nervous system modulates inflammation and epithelial renewal after corneal abrasion through the activation of distinct local macrophages. *Mucosal Immunol*. 2018;11(5):1496–1511.

21. Ferrari G, Bignami F, Giacomini C, Franchini S, Rama P. Safety and efficacy of topical infliximab in a mouse model of ocular surface scarring. *Invest Ophthalmol Vis Sci*. 2013;54(3):1680–1688.
22. Yoeruek E, Ziemssen F, Henke-Fahle S, et al. Safety, penetration and efficacy of topically applied bevacizumab: Evaluation of eyedrops in corneal neovascularization after chemical burn. *Acta Ophthalmol*. 2008;86(3):322–328.
23. Barbariga M, Fonteyne P, Ostadreza M, Bignami F, Rama P, Ferrari G. Substance P modulation of human and murine corneal neovascularization. *Invest Ophthalmol Vis Sci*. 2018;59(3):1305–1312.
24. Amend SR, Valkenburg KC, Pienta KJ. Murine hind limb long bone dissection and bone marrow isolation. *J Vis Exp*. 2016;2016(110):53936.
25. Lasagni Vitar RM, Barbariga M, Fonteyne P, Bignami F, Rama P, Ferrari G. Modulating ocular surface pain through neurokinin-1 receptor blockade. *Invest Ophthalmol Vis Sci*. 2021;62(3):26.
26. Koretsky AP, Silva AC. Manganese-enhanced magnetic resonance imaging (MEMRI). *NMR Biomed*. 2004;17(8):527–531.
27. Lizarbe B, Benitez A, Peláez Brioso GA, et al. Hypothalamic metabolic compartmentation during appetite regulation as revealed by magnetic resonance imaging and spectroscopy methods. *Front Neuroenergetics*. 2013;5:6.
28. Kuo YT, Herlihy AH, So PW, Bell JD. Manganese-enhanced magnetic resonance imaging (MEMRI) without compromise of the blood-brain barrier detects hypothalamic neuronal activity in vivo. *NMR Biomed*. 2006;19(8):1028–1034.
29. Hankir MK, Parkinson JR, Bloom SR, Bell JD. The effects of glutamate receptor agonists and antagonists on mouse hypothalamic and hippocampal neuronal activity shown through manganese enhanced MRI. *Neuroimage*. 2012;59(2):968–978.
30. Shaheen BS, Bakir M, Jain S. Corneal nerves in health and disease. *Surv Ophthalmol*. 2014;59(3):263–285.
31. Labetoulle M, Baudouin C, Calonge M, et al. Role of corneal nerves in ocular surface homeostasis and disease. *Acta Ophthalmol*. 2019;97(2):137–145.
32. Launay PS, Reboussin E, Liang H, et al. Ocular inflammation induces trigeminal pain, peripheral and central neuroinflammatory mechanisms. *Neurobiol Dis*. 2016;88:16–28.
33. Holle D, Katsarava Z, Obermann M. The hypothalamus: Specific or nonspecific role in the pathophysiology of trigeminal autonomic cephalalgias? *Curr Pain Headache Rep*. 2011;15(2):101–107.
34. Herman JP, McKlveen JM, Ghosal S, et al. Regulation of the hypothalamic-pituitary- adrenocortical stress response. *Compr Physiol*. 2016;6(2):603–621.
35. Jänig W, Baron R. Sympathetic nervous system and pain. In: Schmidt R, Willis W, eds. *Encyclopedia of Pain*. Berlin, Heidelberg: Springer; 2007, https://doi.org/10.1007/978-3-540-29805-2_4327.
36. Bernard JF. Hypothalamus and nociceptive pathways. In: Schmidt R, Willis W, eds. *Encyclopedia of Pain*. Berlin, Heidelberg: Springer; 2007, https://doi.org/10.1007/978-3-540-29805-2_1847.
37. Geerling JC, Shin JW, Chimenti PC, Loewy AD. Paraventricular hypothalamic nucleus: axonal projections to the brainstem. *J Comp Neurol*. 2010;518(9):1460–1499.
38. Sharma D, Farrar JD. Adrenergic regulation of immune cell function and inflammation. *Semin Immunopathol*. 2020;42(6):709–717.
39. Marfurt CF, Cox J, Deek S, Dvorscak L. Anatomy of the human corneal innervation. *Exp Eye Res*. 2010;90(4):478–492.
40. Bignami F, Giacomini C, Lorusso A, Aramini A, Rama P, Ferrari G. NK1 receptor antagonists as a new treatment for corneal neovascularization. *Invest Ophthalmol Vis Sci*. 2014;55(10):6783–6794.
41. Liu L, Dana R, Yin J. Sensory neurons directly promote angiogenesis in response to inflammation via substance P signaling. *FASEB J*. 2020;34(5):6229–6243.
42. Barrett-Jolley R, Nunn N, Womack M, Dart C. Function and pharmacology of spinally-projecting sympathetic preautonomic neurones in the paraventricular nucleus of the hypothalamus. *Curr Neuropharmacol*. 2011;9(2):262–277.
43. Watkins ND, Cork SC, Pyner S. An immunohistochemical investigation of the relationship between neuronal nitric oxide synthase, GABA and presympathetic paraventricular neurons in the hypothalamus. *Neuroscience*. 2009;159(3):1079–1088.
44. Womack MD, Morris R, Gent TC, Barrett-Jolley R. Substance P targets sympathetic control neurons in the paraventricular nucleus. *Circ Res*. 2007;100(11):1650–1658.
45. Feetham CH, Barrett-Jolley R. NK1-receptor-expressing paraventricular nucleus neurones modulate daily variation in heart rate and stress-induced changes in heart rate variability. *Physiol Rep*. 2014;2(12):e12207.
46. Figueira L, Janeiro C, Ferreirinha F, et al. Regulation of corneal noradrenaline release and topography of sympathetic innervation: functional implications for adrenergic mechanisms in the human cornea. *Exp Eye Res*. 2018;174:121–132.
47. Figueira L, Ferreira C, Janeiro C, Serrao P, Falcao-Reis F, Moura D. Concentration gradient of noradrenaline from the periphery to the centre of the cornea—a clue to its origin. *Exp Eye Res*. 2018;168:107–114.
48. Pavlov VA, Tracey KJ. The vagus nerve and the inflammatory reflex—linking immunity and metabolism. *Nat Rev Endocrinol*. 2012;8(12):743–754.
49. Tracey KJ. The inflammatory reflex. *Nature*. 2002;420(6917):853–859.
50. Donello JE, Guan Y, Tian M, et al. A peripheral adrenoceptor-mediated sympathetic mechanism can transform stress-induced analgesia into hyperalgesia. *Anesthesiology*. 2011;114(6):1403–1416.
51. Yun H, Lathrop KL, Hendricks RL. A central role for sympathetic nerves in herpes stromal keratitis in mice. *Invest Ophthalmol Vis Sci*. 2016;57(4):1749–1756.
52. Wang Y-J, Li X-F, Ding F, et al. Noradrenaline regulates substance P release from rat dorsal root ganglion neurons in vitro. *Neurosci Bull*. 2011;27(5):300–306.
53. K E, N S. Stress-induced release of substance P in the locus coeruleus modulates cortical noradrenaline release. *Naunyn Schmiedebergs Arch Pharmacol*. 2007;376(1–2):73–82.
54. Maryanovich M, Takeishi S, Frenette PS. Neural regulation of bone and bone marrow. *Cold Spring Harb Perspect Med*. 2018;8(9):a031344.
55. Hefco V, Olariu A, Hefco A, Nabeshima T. The modulator role of the hypothalamic paraventricular nucleus on immune responsiveness. *Brain Behav Immun*. 2004;18(2):158–165.

Investigative Ophthalmology & Visual Science